

# Measurements of timing resolution of ultra-fast silicon detectors with the SAMPIC WTDC

D. Breton<sup>a</sup>, V. De Cacqueray<sup>b,1</sup>, E. Delagnes<sup>b</sup>, H. Grabas<sup>c</sup>, J. Maalmi<sup>a</sup>,  
N. Minafra<sup>d,2</sup>, C. Royon<sup>e</sup>, M. Saimpert<sup>b,\*</sup>

<sup>a</sup>*CNRS/IN2P3/LAL Orsay, Université Paris-Saclay, F-91898 Orsay, France*

<sup>b</sup>*IRFU, CEA, Université Paris-Saclay, F-91191 Gif-sur-Yvette, France*

<sup>c</sup>*Santa Cruz Institute for Particle Physics UC Santa Cruz, CA 95064, USA*

<sup>d</sup>*Dipartimento Interateneo di Fisica di Bari, Bari, Italy, CERN, Geneva, Switzerland*

<sup>e</sup>*University of Kansas, Lawrence, USA*

---

## Abstract

The SAMpler for PICosecond time (SAMPIC) chip has been designed by a collaboration including CEA/IRFU/SEDI, Saclay and CNRS/LAL/SERDI, Orsay. It benefits from both the quick response of a time to digital converter (TDC) and the versatility of a waveform digitizer to perform accurate timing measurements. Thanks to the sampled signals, smart algorithms making best use of the pulse shape can be used to maximize time resolution. A software framework has been developed to analyse the SAMPIC output data and extract timing information by using either a constant fraction discriminator or a fast cross-correlation algorithm. SAMPIC timing capabilities together with the software framework have been tested using Gaussian signals generated by a signal generator or by silicon detectors pulsed with an infra-red laser. Under these ideal experimental conditions, the SAMPIC chip has proven to be capable of timing resolutions down to 4 (40) ps with synthesized (silicon detector) signals.

*Keywords:* ASIC, Time-of-flight, Time to digital converter, Waveform sampling, Time resolution, Silicon detector

---

---

\*Corresponding author.

*Email address:* [matthias.saimpert@cern.ch](mailto:matthias.saimpert@cern.ch) (M. Saimpert)

<sup>1</sup>now at: *LSCE, CEA, Université Paris-Saclay, F-91191 Gif-sur-Yvette, France.*

<sup>2</sup>now at: *University of Kansas, Lawrence, USA.*

## 1. Introduction

At the Large Hadron Collider (LHC) at CERN [1], which is the highest energy proton-proton collider in the world with a center-of-mass energy of 14 TeV, special classes of events can be studied where protons are found to be intact after collisions. These events are called “diffractive” in the case of gluon exchanges. They can also originate from photon exchanges as well and then called photon-induced processes. The physics motivation for their study is a better understanding of diffraction in terms of QCD [2, 3] and the search for physics beyond standard model such as the existence of extra-dimensions via anomalous couplings between photons,  $W$  and  $Z$  bosons [4, 5, 6, 7, 8, 9].

The intact protons scattered at small angles can be measured using dedicated detectors hosted in roman pots, a movable section of the vacuum chamber that can be inserted a few millimeters away from the beam at more than 200 m from each side of the main central ATLAS [10] or CMS [11] detectors. In order to measure rare events at the LHC, the luminosity (*ie.* the number of interactions per second) has to be as large as possible. In order to achieve this goal, the number of interactions per bunch crossing is planned to be very large, up to 40-70 during the second LHC run (2015-2018). The projects aiming to measure intact protons at high luminosity in the ATLAS and CMS/TOTEM [12] experiments are called respectively AFP (ATLAS Forward Proton detector) [13] and CT-PPS (CMS/TOTEM-Precision Proton Spectrometer) [14, 15].

In this context, timing measurements are crucial in order to determine if the intact protons originate from the main hard interaction or from secondary ones, called pileup interactions in the following. Measuring the arrival time of protons with a typical precision of 10 ps RMS allows to discriminate between hard interaction vertices and pileup interactions up to a precision of about  $\pm 2$  mm. For 40 interactions occurring in the same bunch crossing at the LHC, such a precision on time-of-flight measurements leads to a background reduction by a factor close to 40 [16].

Timing measurements have also many other applications, for example in medical imaging. Indeed, PET imaging would highly benefit from 10 ps timing precision [17]: first, most of the fake coincidences could be suppressed, which would lower the amount of data to be recorded; second, depending on the signal over noise ratio (SNR) achieved, offline image reconstruction could be no longer necessary and real time image formation could be performed. This would allow to reduce the exposure of the patient to the radioactive

tracer and to be able to repeat immediately the tomography if needed.

The SAMPIC chip [18] has been designed to achieve a 5 ps RMS timing precision. In this paper, the second SAMPIC release is used (called V1), and we present the results of various tests carried out using Gaussian signals synthesized by a signal generator and silicon detectors pulsed by an infrared laser. The analysis is performed with a dedicated software framework developed to analyse SAMPIC data.

In Section 2, we give a simple description of the SAMPIC chip, stressing the advantages with respect to previous technologies. Section 3 is dedicated to a detailed description of the hardware and the online software used to acquire data. The offline software used for timing reconstruction is presented in Section 4 while the tests of the SAMPIC chip are presented in Section 5, first with synthetic signals and then using fast silicon detectors. Finally, a summary of the SAMPIC performances measured in this paper is reported in Section 6.

## 2. The SAMPIC chip

### 2.1. TDCs

Current systems usually rely on Time to Digital Converters (TDC) to measure precise timing. TDCs use a counter that provide coarse timing associated with a Delay Locked Loop doing a finer interpolation of the latter. The timing resolution is then often limited by the DLL step and with most advanced Application Specific Integrated Circuit (ASICs) one can achieve a resolution of about 20 ps RMS.<sup>3</sup>

An additional drawback of this technique for analog pulses (such as the ones produced in a typical particle detector) is that the TDC relies on a digital input signal. Therefore, one needs first to convert the signals prior to any measurement. That conversion is typically done using a fast discriminator. However, the amplitude dispersion of the signal may induce time walk effects on the digital output signal, even if they are usually corrected via time over threshold measurements. Furthermore, the discriminator introduces an additional jitter to the system since it impacts directly the measurement. The timing resolution of such a system is then given by the quadratic sum of the TDC and the discriminator resolution.

---

<sup>3</sup>new developments at CERN target 5 ps [19].

## 2.2. Waveform TDC

To overcome this limitation, a new approach has been proposed, based on the innovative principle of a waveform-based TDC (WTDC). In such a system an analog memory is added in parallel with the delay line. The memory is used to sample the input signal which can now be analog. It also allows to perform an interpolation of the samples recorded on the latter. A discriminator is anyhow present, but only used to assert a trigger signal and therefore not anymore in the critical timing path. Time information is ultimately given by the association of three measurements:

**Coarse counter:** upon triggering, the state of a 12-bit Gray counter connected to the DLL clock is recorded and appended to the data read-out.

**DLL step:** the position of the trigger within the 64 steps of the DLL is recorded as well and can be used to define a region of interest.

**Digital treatment:** interpolation or other more sophisticated processing of the digitized waveform samples allows to reach an RMS time resolution of a few picoseconds.

## 2.3. SAMPIC architecture

SAMPIC[18] implements the WTDC approach in an ASIC for 16 independent input channels. A basic schematic of one SAMPIC channel is shown in Figure 1.

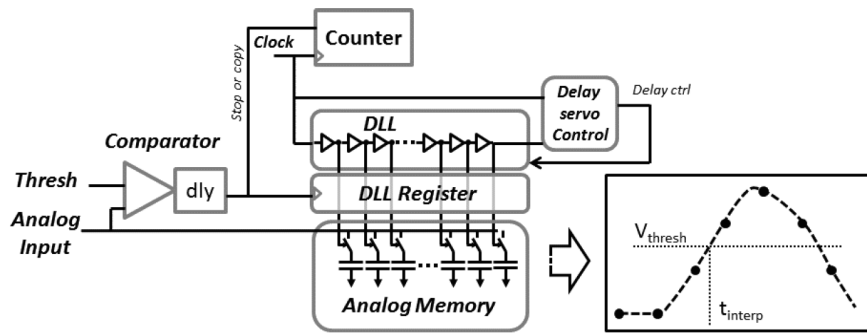


Figure 1: Schematic of one channel of the SAMPIC WTDC.

For each channel the input signal (50  $\Omega$ -terminated on-board, AC coupled) is sent to both:

**64 sampling cells:** signal sampling is controlled by a ASIC-global DLL. Upon channel trigger, the 64 samples are frozen and digitized in parallel using Wilkinson ADCs over up to 11 bits.

**A discriminator:** sampling for each channel can be stopped and held by a dedicated discriminator or by an external trigger signal. A variable delay can be added to the output of the discriminator in order to keep additional samples after threshold crossing. The discriminator threshold can be adjusted independently for each channel.

Upon channel triggering, the state of the Gray counter, the position of the DLL strobes and the 64 analog samples are latched. During data readout the counter value and DLL position are appended to the digital samples values.

The fact that SAMPIC makes use of a Wilkinson ADC structure has obvious advantages in terms of power consumption and linearity, but it induces a noticeable dead-time per channel due to the conversion. The latter currently varies as a function of the desired accuracy from less than 200 ns for an 8-bit conversion to 1.3  $\mu$ s for an 11-bit one. The conversion range can be adjusted with respect to the signal amplitude in order to get the best trade-off between dead-time and time precision.

The dead-time per channel got the possibility to be reduced to about 50 ns for one following event in the new version of SAMPIC (V2, released in December 2015), by using the so called “ping-pong” method which permits using two channels to store two closely consecutive events. This technique was first implemented on a pair of ARS chips for the ANTARES experiment [20]. As a reference, we show a summary of the main characteristics of SAMPIC V1 in Table 1.

SAMPIC is also fairly cheap (about 10 Euros per channel) with respect to competing technologies, which cost usually a few 1000s Euros per channel when such a precision is reached (commercial modules). Therefore, SAMPIC can be used in principle in large scale detectors.

More details about SAMPIC integration are given in Section 3.

	Performances measured
Technology	AMS CMOS 0.18 $\mu$ m
Number of channels	16
Power consumption	180 mW (1.8 V supply)
Capacitor array depth	64
Discriminator noise	2 mV
Sampling speed	1.6 - 8.4 GSa/s <sup>4</sup>
3dB Input bandwidth	1.6 GHz
ADC precision	8 to 11 bits <sup>5</sup>
Noise	< 1.3 mV RMS
Input dynamic range	1 V (0.1 V to 1.1 V)
Conversion time	200 ns on 8 bits - 1.6 $\mu$ s on 11 bits
Readout time	37.5 ns + 6.25 ns/sample at 160 MHz <sup>6</sup>
Time precision before calibration	15 ps RMS
Time precision after calibration	< 5 ps RMS

Table 1: Table of SAMPIC main performances.

<sup>4</sup>Up to 10.2 GSa/s on the 8 first channels.

<sup>5</sup>Trade-off time vs resolution.

<sup>6</sup>A readout up to 200 Mhz is possible.

### 3. Acquisition board and control software

The SAMPIC chip is integrated in an *out-of-the-box* configuration that includes one or two mezzanine boards embedding the chip, plugged on a motherboard permitting its control and readout. A software in charge of controlling the acquisition, displaying and saving data is also available. The software also allows to perform real-time measurements on the signals.

The full device, shown in Figure 2, requires a simple 5 V power supply and a PC that can be connected through USB 2.0, Gigabit Ethernet or optical fibre. Moreover, it is possible to supply an external clock and some control signals, for instance to setup an external trigger or a signal that vetoes the trigger. The device has 16 or 32 MCX connectors for the analog input, depending on the number of SAMPIC chips used (1 or 2).



Figure 2: Picture of the SAMPIC chip and its acquisition board in the 16-channel version.

The control software is available for Windows platforms and based on LabWindows libraries. A multi-platform version is also under development. The main parameters that can be set using the software are:

**Sampling parameters:** sampling frequency (from 1.6 to 10.2 GS/s), baseline (from 0.1 to 1.1 V), Analog to Digital conversion range (8, 9, 10 or 11 bits).

**Trigger parameters:** trigger mode (see section 2), thresholds and polarity of the signal.

**Acquisition parameters:** data format (ASCII or binary) and maximum file size, length of the acquisition (time or number of hits).

Moreover, it is possible to correct the acquired data through the control software [18]. The two types of calibration which have to be performed are implemented: the first one concerns the ADC linearity of each cell, which is measured via 20 DC measurements along the baseline range. The first or second order polynomial that best fits the deviation from the expected values is then used to compensate for the non linearities. The delay line between the cells of the analog memories are also affected by non uniformities which directly affect the time spacing of the samples. The calibration procedure applicable to SAMPIC V1 to correct for those non uniformities requires to send an externally generated sine wave to each channel. The wave is then sampled and used to precisely measure the delays between the cells. In the new version of the chip (V2, released in December 2015), the sine wave generator is directly integrated inside the chip so that no external signals should be required any longer.

The calibration procedure needs to be repeated for each set of acquisition parameters (*i.e.* sampling frequency and number of ADC bits). The software takes care of storing the configuration parameters for all the different acquisition scenarios and makes use of them to correct the acquired data. It should be noted that without time calibrations, the SAMPIC chip is still able to achieve a very precise time resolution, of the order of 15 ps RMS at 6.4 GS/s [18].

Finally, the software can also be used to display acquired data and to perform some preliminary analysis. For instance, it is possible to measure the RMS noise for selected channels and to compute online the time difference between two channels via basic algorithms without any pre-processing (CFD or fixed threshold).

## 4. Offline software

### 4.1. Data format definition

The data acquired using the SAMPIC chip are processed by the FPGA located on the acquisition board and can be saved in a binary or ASCII file using the control software. A preliminary estimation of the time differences can be made online using the control software. However, an offline analysis

is very useful to compare easily several time algorithms and implement some data cleaning and/or pre-processing if required during the development stage.

The offline software is a C++ code based on the ROOT framework.<sup>7</sup> First, the sampled waveforms are extracted from the data acquired with the online software and stored in a hierarchical structure (TTree). Data are then organized by *events*. If an external trigger is provided, two or more hits are considered belonging to the same event when the differences between the channel and the trigger timestamps are smaller than  $\Delta t_{max}$ , after being corrected for a fixed trigger latency. Otherwise, all coincident hits, *ie.* with a time difference between their respective starting time less than  $\Delta t_{max}$ , are recorded in the same event. The value of  $\Delta t_{max}$  has to be set by the user. A small value ( $\sim 20$  ns) is generally used when high rate is expected whereas a larger value is preferable otherwise in order to ensure some tolerance, for example when one uses cables with different lengths for the analog input.

For each acquisition the baseline, *ie.* the average sampled voltage when no event occurs, is measured from the first  $n_b$  recorded points, where  $n_b$  must be specified by the user. The baseline is then recorded in the data tree. Other relevant information, such as sampling period, channel number and ADC counts are also saved. This intermediate step is useful to disentangle the data acquisition from the analysis part, foreseeing the usage of the same analysis code for future version of the hardware and with third part sampling devices such as, for example, an oscilloscope.

#### 4.2. Time measurement analysis

Two main time reconstruction algorithms can then be run on the data tree from the offline software:

- Constant Fraction Discriminator (CFD) [21].
- Cross-Correlation (CC) [22].

The most common approach to compute the time of arrival of a sampled signal is to use a CFD algorithm [21]. The arrival time is then defined as the instant when the signal crosses the threshold corresponding to a given fraction of the signal amplitude, which needs to be set by the user beforehand. This threshold definition makes the results almost independent from the signal amplitude (suppression of the time walk effect). The threshold crossing

---

<sup>7</sup><https://root.cern.ch/>

value is obtained by using a linear interpolation of the sampled points (then based on 2 points) and the signal amplitude is retrieved from a parabola interpolation (then based on three points).

The theoretical uncertainty from a CFD timing measurement can be evaluated with the following equation [21]:

$$\sigma_{\text{CFD}}^2 = \left( \sigma_{\text{noise}} \cdot \frac{\tau}{A} \right)^2 + \sigma_{\text{jitter}}^2, \quad (1)$$

where  $\sigma_{\text{CFD}}$  is the CFD total uncertainty,  $\sigma_{\text{noise}}$  is the RMS noise of the channel,  $\frac{\tau}{A}$  is the rising time divided by the signal amplitude and  $\sigma_{\text{jitter}}$  represents the uncertainty on the time of each recorded sample intrinsic to each channel of the chip. However, the formula of Equation 1 assumes the rising edge of the signal to be linear ( $\frac{\tau}{A}$ ), which is usually not entirely true. It is still very useful to compare the measurements with theoretical expectations from an ideal signal with a linear rising edge, as we will see in Section 5.

A refined version of the CFD algorithm has also been implemented in the software, consisting by averaging the times returned by multiple CFDs with different ratios. In case more than two points are available along the rising edge, this technique often improves the resolution by using the timing information carried by more samples than the classic CFD implementation. The computation time is then slightly increased, but still of the order of 1 ms per event.<sup>8</sup>

The alternative method is based on the cross-correlation algorithm [22]. A correlation function is computed between the acquired signal and a template extracted from an independent set of acquisition with high statistics. The maximum of this function obtained by varying the time shift between the signal and the template indicates the optimal superposition of the two which can then be used to determine the timing of the original signal.

This technique requires the generation of templates for the expected signals, which might not be straightforward for certain application with relatively high statistical fluctuations of the signal like particle detection with thin detectors. However, if the fluctuations stay reasonable, the CC allows to take the maximum benefit from the whole sampling points. The main steps performed by the cross-correlation algorithm can be summarized as follows:

- A template is generated for each channel using independent, high statis-

---

<sup>8</sup>Computation performed with a 2.3 GHz processor including a 4 Gb memory.

tics data samples acquired with the same experimental apparatus and conditions similar to the data to be analysed. Baselines are removed and all signals are normalized to their amplitudes and synchronized using a CFD algorithm. The templates are then computed channel by channel by averaging all signal shapes.

- For each hit to be analysed, a coarse synchronization between the signal and the template is first done using a standard CFD.
- The template is then translated over the signal until the correlation function reaches a maximum. In order to reduce the computation time, a limited translation window is selected around the coarse synchronization done previously.
- The optimal time shift between the signal and the template is found for each hit of the event and recorded.

The advantage of the cross-correlation method is that the information from all the sampled points can be included in the computation whereas the CFD uses only a few points by definition, *i.e.* the ones close to the maximum and the ones close to the threshold crossing. Moreover, the CC should not be biased by an inaccurate baseline subtraction on an event-by-bin basis<sup>9</sup> and the correlation function value at maximum could in principle be used as a data quality estimator.

However, the reproducibility of the signal affects directly the performance of the algorithm. Therefore, only a sub-range of points showing small statistical fluctuations are usually included in the signal-template scan, such as all points ranging from 10% to the maximum of the signal along the rising edge. It should be noted also that the computation time of the CC algorithm is significantly higher than for the CFD algorithm by about a factor 100.

In conclusion, the offline software is able to measure the time difference between two signals within one event or with respect to an external reference via various signal algorithms. For the CC algorithm, the signal-template synchronization is also recorded in the output. In the tests presented in the next section, the time difference between the signals is fixed and the measurement with SAMPIC is repeated a large number of time under similar

---

<sup>9</sup>Only the templates could be biased by the baseline subtraction. However, since it is averaged over a large statistics sample the effect should be greatly reduced.

conditions. The spreading of the measurement, *ie.* the RMS of the histogram filled with the various measurements, then corresponds to the time resolution of the acquisition chain and may be used to measured the performance of the acquisition chain. In Section 5, the experimental results are reported.

## 5. Experimental measurements

Different tests were undertaken to measure SAMPIC performance and compare the results of the various algorithms implemented in the offline software. First, some preliminary tests done using signal synthesized by a signal generator are reported in Section 5.1. Then in Section 5.2, the SAMPIC chip and offline software are tested together with ultra-fast silicon detectors (UFSDs) [23, 24] pulsed by an infra-red laser beam. The UFSDs are new generation silicon detectors being developed at INFN, Torino, UC Santa Cruz and the Institute of Microelectronics of Barcelona for fast timing application. More details will be given in Section 5.2.

### 5.1. Tests with signal generator

Preliminary tests of the SAMPIC chip are done using signals from a LeCroy pulse generator.<sup>10</sup> Those signals are used to characterize the chip and to investigate the performance of the various algorithms under ideal conditions. The generator is configured to produce Gaussian pulses with a rise time smaller than 1 ns and a width of 0.90 ns at a rate of 1 kHz. The amplitudes of the signals are reduced using several broadband attenuators (Wavetek, 3 GHz) and then split by a T-junction. Finally, the signals are sent to two different channels of SAMPIC through cables of different length in order to create a sizable delay between them. The jitter between the two signals is assumed to be less than 1 ps when they enter the chip.

The sampling frequency of SAMPIC is set to 6.4 GS/s for the entire test. SAMPIC channels are in self-trigger mode with a threshold set according to the incoming signal amplitude. During the first series of tests, the delay between the two signals is fixed to about 5 ns while the signal amplitude is reduced progressively using the attenuators (*amplitude test*). During the second series of tests, the amplitude of the LeCroy pulse is fixed to 1.2 V while the delay between the two signals acquired by the SAMPIC chip is varied from a few picoseconds to a few hundreds of nanoseconds (*delay test*).

---

<sup>10</sup>LeCroy 9211 – 250 MHz.

Examples of signals acquired by one of the SAMPIC channels from 27 dB-reduced Lecroy pulses ( $\simeq 33$  mV amplitude) are shown in Figure 3. Some reflections of the pulse are observed due to the non perfect coupling at the connection points because no adaptation of impedance is performed when splitting the original signal (T-junction). Due to the limited bandwidth of the cables and skin effect, we also noticed an attenuation of the signal at high delay ( $> 100$  ns) by up to 30% due to large cable length (delay test).

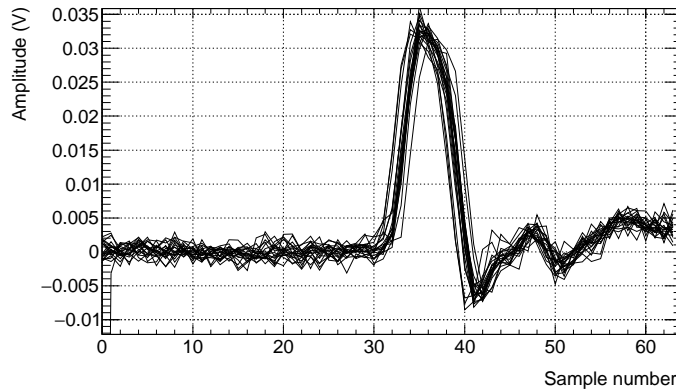


Figure 3: Several signals with an amplitude of 33 mV acquired using the SAMPIC chip sampling at 6.4 GS/s are shown. The signals are produced using a Gaussian pulse generator and interpolated linearly for plotting purposes. The strong overlap of the various curves shows the very good reproducibility of the signals. The first point is sometimes lost, which is a known feature of the chip related to SAMPIC architecture.

For each data sample, 10,000 events are processed using the offline software (section 4) using both the CFD and the cross-correlation algorithm to reconstruct the time difference between the two channels. The default CFD is configured to use a threshold at 50% of the amplitude. A refined CFD algorithm averaging the results obtained with thresholds at 30%, 35%,  $\dots$ , 70% of the amplitude is also performed. Furthermore, an example of synchronization between a template and a signal using the cross-correlation algorithm is shown in Figure 4.

The histograms of the 10,000 time differences measured with the proposed methods are shown in Figure 5 for signals of 33 mV (top) and 660 mV amplitudes (bottom) delayed by about 5 ns (delay test). The Root Mean Squares (RMS) of the time difference distributions obtained for the various amplitudes are shown in Figure 6. The RMS is about 4 to 6 picoseconds for high amplitudes ( $> 200$  mV), which correspond to data with a good

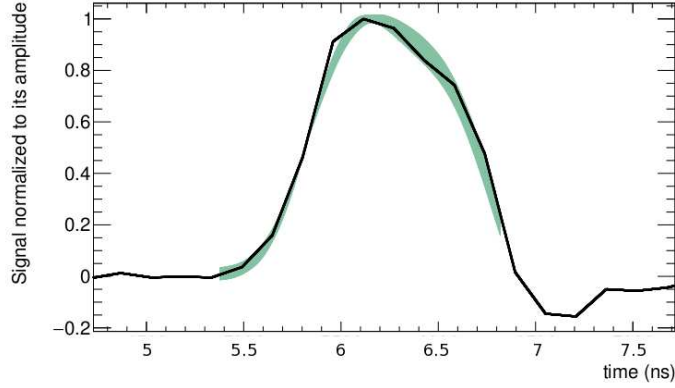


Figure 4: Synchronization performed between a template (band) and a signal (line) by the cross correlation algorithm. The band of the template corresponds to its statistical dispersion (RMS). It reaches zero at the point used to synchronize the different signals together when building the template (see Section 4). The signal corresponds to one of the sampling shown in Figure 3.

Signal over Noise Ratio (SNR). However, the RMS increases significantly for amplitudes below 100 mV because of the low SNR. In this region, the cross-correlation improves significantly the resolution, up to a factor close to 2. However the refined CFD does not provide any significant resolution improvement, most likely because no more than 1 or 2 points are recorded along the rising edge for those very fast signals but also because the time walk effect is probably very small thanks to the good regularity of the pulse amplitudes.

The experimental results for the CFD with a fraction of 0.5 are in good agreement with the theoretical predictions from Equation 1 for those ideal (very fast) signals, except at very low SNR where non-linearities in the rising edge may occur.<sup>11</sup> The predictions are computed using the observed RMS noise in each channel, which is about 1.2 mV in both cases. The jitter value on the time difference is set to match the predictions to the measurement at high SNR and is found to be about 4 ps RMS. If both channels are uncorrelated, this is equivalent to a  $4/\sqrt{2} \simeq 3$  ps resolution per channel. Since small correlations could arise because the same chip is used for both measurement,

---

<sup>11</sup>The theoretical predictions are computed for a time difference between two channels, *ie.*  $\Delta t = t_1 - t_2$  with Equation 1 applying for each of the two terms.

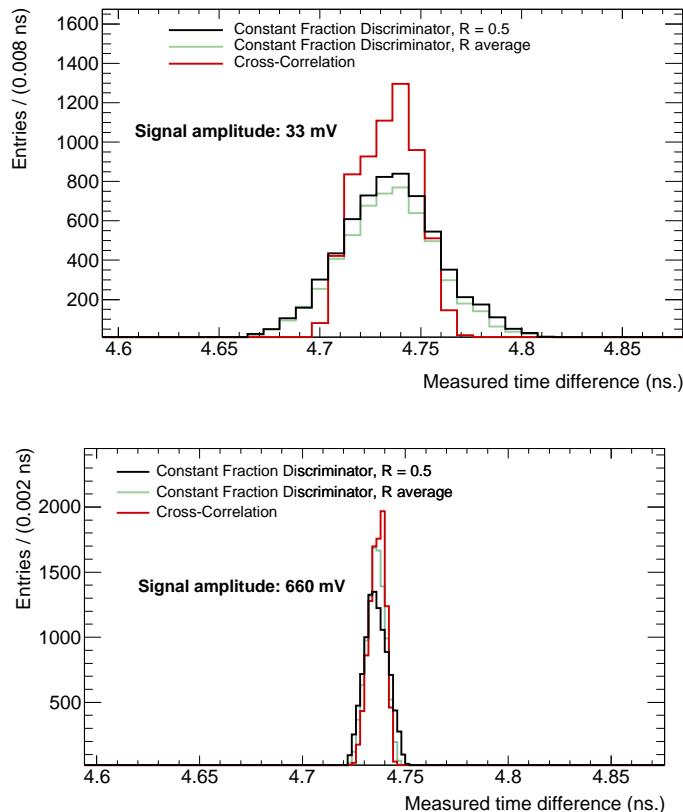


Figure 5: Time difference distributions for 10,000 events between two signals of 33 mV (top) and 660 mV (bottom) amplitude delayed by about 5 ns. The distributions obtained from the three algorithms implemented in the offline software are shown.

we only quote the RMS on a  $\Delta t$  measurement (4 ps). This very low value validates the SAMPIC design, which aimed for a jitter below 5 ps RMS (see Section 2).

In addition, the RMS has a very small dependence on the delay between the signals (delay test), as shown in Figure 7. The small increase of the RMS observed in the Figure is attributed to the attenuation of the signal by longer cable lengths as mentioned previously.

Hence, under those ideal conditions, the SAMPIC chip shows an excellent intrinsic resolution of about 4 ps for signal amplitudes of 0.4 V, in agreement with the design goal. Moreover, the cross-correlation algorithm achieves significantly better performances for signals with low SNR with re-

spect to the CFD. In Section 5.2, the tests performed using ultra-fast silicon detectors are presented.

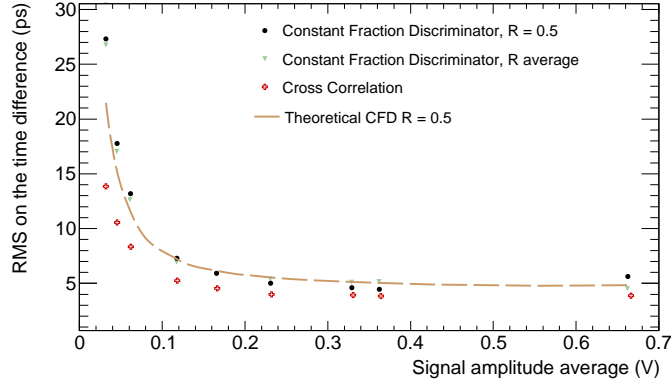


Figure 6: RMS of the time difference between two signals measured from 10,000 events by the SAMPIC chip at 6.4 GS/s, with respect to the signal amplitude (amplitude test). The time difference is fixed at about 5 ns.

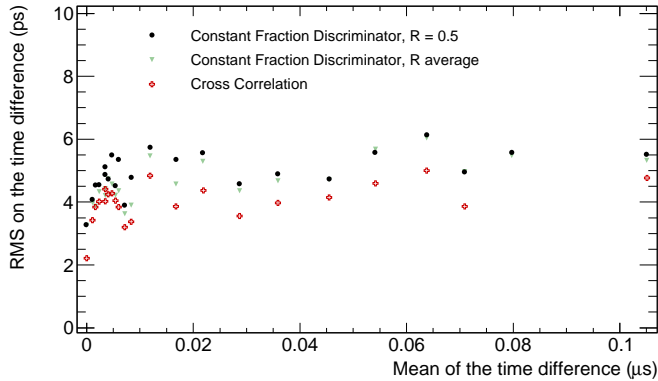


Figure 7: RMS of the time difference between two signals measured from 10,000 events by the SAMPIC chip at 6.4 GS/s, with respect to the mean delay (delay test). The signal amplitude is fixed at about 660 mV.

### 5.2. Tests with ultra-fast silicon detectors

In order to test the SAMPIC chip and the offline software with signals generated by real particle detectors, a particular design of Low Gain Avalanche

Diodes-based detectors (LGAD) are used [25] called ultra-fast silicon detectors (UFSDs) [23, 24]. Low Gain Avalanche Diodes (LGAD) are a novel type of silicon detectors that combines the advantages of internal gain, as in avalanche photo-diodes (APDs), with the properties of standard silicon detectors. The key idea is that low gain will not generate dark counts and excessive leakage current as it happens in APD, but will offer an enhanced signal that can be used for timing applications. Starting from this idea, Ultra-Fast Silicon detectors were proposed, optimizing the LGAD idea for timing measurements.

### 5.2.1. First setup

In the first instance, two UFSDs are fired using an infra-red laser and amplified by commercially available amplifiers. The setup is the following :

- A 1060 nm picosecond laser beam<sup>12</sup> is split and sent to two UFSDs through optical fibres. The laser has a bandwidth of 2 nm and includes a tunable amplitude. The jitter between the two laser pulses is assumed to be very negligible.
- Ultra-fast silicon detectors of gain 10 [24, 26] polarized with a voltage of 800 V are used.
- The signals are amplified with CIVIDEC<sup>13</sup> C2 broadband amplifiers (BDA). A C6 fast charge sensitive amplifier (CSA) will be used for the second part of the tests.
- The two active SAMPIC channels are configured to sample data at 6.4 GS/s (C2-BDA) or 3.2 GS/s (C6-CSA).
- Data is acquired on a computer and processed by the offline analysis software.

A picture of the first experimental setup is shown in Figure 8. BDAs read the currents generated by the detectors on their amplified input resistance ( $50\ \Omega$ ) and amplify them of 40 dB.

The laser beam intensity is varied in a range corresponding to various energy deposits, *ie.* from 2 to 4 Minimum Ionizing Particles (MIPs). This

---

<sup>12</sup>PiLas PiL106X.

<sup>13</sup><http://www.cividec.at/>

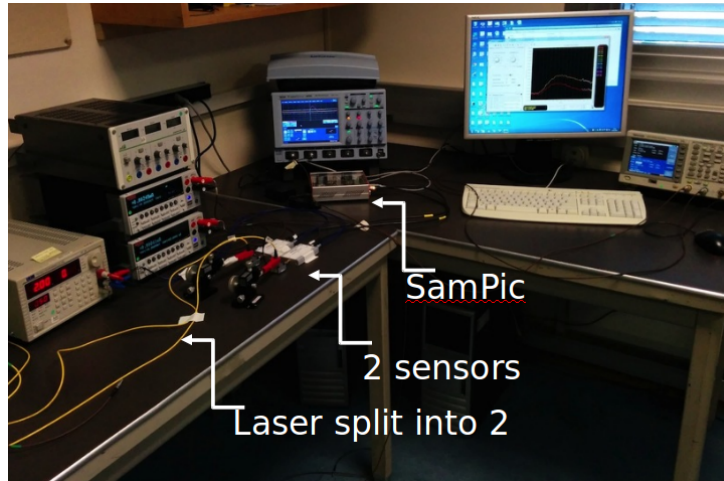


Figure 8: Test bench at CERN (June 2014). Ultra-fast silicon detectors of gain 10 and CIVIDEC C2-BDA amplifiers are used together with the SAMPIC WTDC.

variation accounts roughly for the Landau distribution that one would obtain from high energy particles. However, the amplification is not high enough to get a sizable signal from an energy deposit corresponding to 1 MIP.

Examples of signals acquired with a laser intensity corresponding to about 2 MIPs are shown in Figure 9. The polarity of the signal is inverted because of the UFSD charge carriers. The acquisition window is centred on the first edge of the pulse. An example of synchronization by cross-correlation between a signal and the corresponding template is shown in Figure 10.

The time difference distributions for 10,000 events according to the various algorithms are shown in Figure 11 whereas the dependence of the RMS of the measured time difference with respect to the amplitude of the signals is shown in Figure 12. The measured resolutions are always below 110 ps. The RMS obtained from the refined CFD algorithm (R average) improves the resolution by up to 20 ps with respect to the standard one ( $\simeq 15\%$ ) and gets closer to what one would expect from a standard CFD performed on signals rising linearly (labelled as theoretical CFD). This is most likely due to the fact that much more points are sampled on the rising edge than before, the signals being much slower.

The theoretical expectations are computed from Equation 1 using the noise RMS as observed in data, which is found to be slightly higher than in the previous test ( $\simeq 1.4$  mV), most likely because of the additional noise

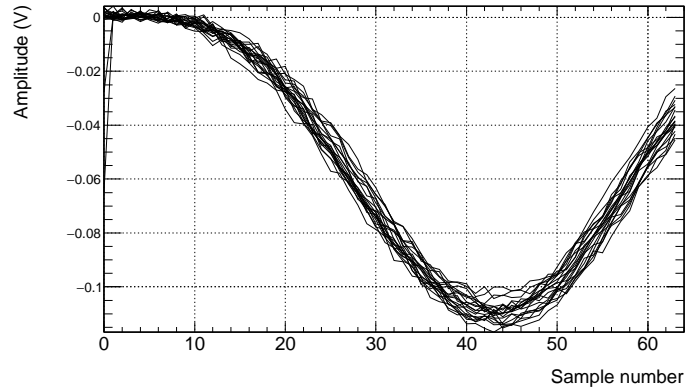


Figure 9: Signals generated by a USFD amplified with a CIVIDEC C2-BDA amplifier and acquired by the SAMPIC chip sampling at 6.4 GS/s. Signal properties: 3.5 ns rise time (measured within 10-90% of the signal amplitude),  $\sim 2$  MIPs laser intensity ( $\simeq 110$  mV in SAMPIC). The signals are interpolated linearly for plotting purposes. The first point is sometimes lost, which is a known feature of the chip related to SAMPIC architecture.

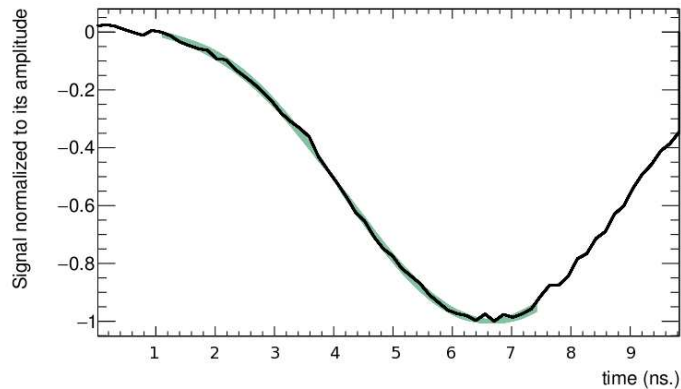


Figure 10: Example of synchronization performed between a template (band) and a signal (points) by the cross correlation algorithm. The error band of the template corresponds to its statistical dispersion. The signal corresponds to one of the signals described in Figure 9.

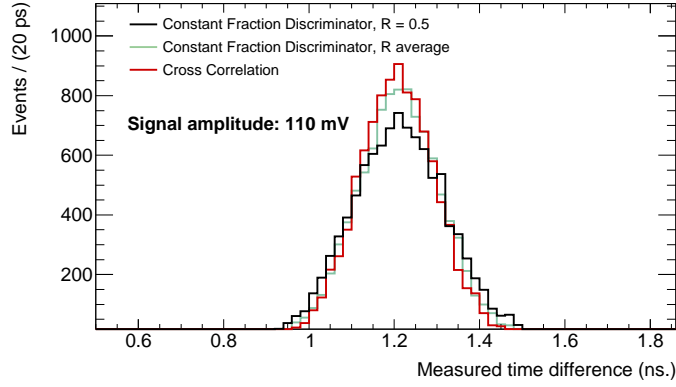


Figure 11: Time difference distributions corresponding to 10,000 signals from C2-BDA-amplified USFDs of 110 mV of amplitude ( $\sim 2$  MIPs). Results for the three algorithms implemented in the offline software are shown.

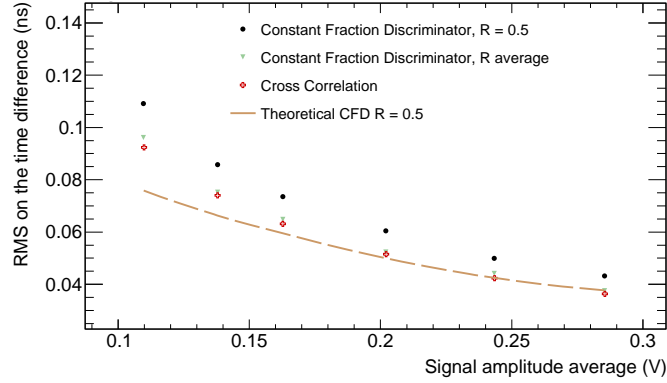


Figure 12: RMS on the time difference between two signals from C2-BDA-amplified USFDs acquired 10,000 times by the SAMPIC chip at 6.4 GS/s with respect to the signal amplitude. Signal amplitudes are varied by tuning the laser intensity to mimic an amplitude corresponding from  $\sim 2$  to 4 MIPs.

coming from the USFD + BDA. This time, the jitter value is dominated by the detector + amplification system ( $\simeq 30$  ps) and spoils significantly the measurement resolution. The CC algorithm gives results very close to the refined CFD and slightly better, which is attributed to the fact that the tails of the signals are excluded from the correlation function due to too high fluctuations. Similarly to the previous tests, the resolution seems to stabilize for amplitudes greater than 300 mV.

### 5.2.2. Second setup

A second campaign of tests was carried out in October 2014 in the INFN laboratories in Turin. It aimed to measure the timing resolution of a single SAMPIC channel, whereas in previous tests only the resolution on the time difference between two channels could be accessed.

For this purpose, one SAMPIC channel is dedicated to the acquisition of the trigger signal of the laser, whereas the other one acquires a UFSD signal. Since the trigger signal is very fast and with a high SNR, its time jitter can be considered negligible with respect to the one of the silicon detector. Consequently, the measurements performed in the following evaluates the SAMPIC single channel resolution directly.

Furthermore, for this test the detector is read using a CIVIDEC C6-CSA amplifier so that the laser intensity can be correctly tuned to mimic from 1 to 4 MIP energy deposits. Signals after amplification range from 120 to 480 mV. Under those conditions, the rise time of the signal sent to SAMPIC is much longer and close to 6 ns (if measured between 10% and 90% of maximum). The SAMPIC sampling frequency is therefore decreased to 3.2 GS/s in order to adjust the acquisition time window.

The signal shape is shown in Figure 13. Similarly to the previous tests, the acquisition window of SAMPIC is centered on the pulse rising edge. The resolution obtained for different signal amplitudes is shown in Figures 14. One can see that SAMPIC is able to provide timing measurements up to 85 ps resolution for signals corresponding to 1 MIP, *ie.* 120 mV amplitude in this case. In this region, the cross-correlation algorithm allows to improve the resolution by 20 ps ( $\simeq 17\%$ ) compared to a standard CFD algorithm and by 10 ps compared to the refined CFD. At higher signal-over-noise ratio, SAMPIC can perform measurements with a resolution up to 40 ps whereas the signal rises in 6 ns. As for the previous test, the resolution plateau seems to be reached for amplitudes greater than 300 mV. In the latter case, the different algorithm performance becomes similar.

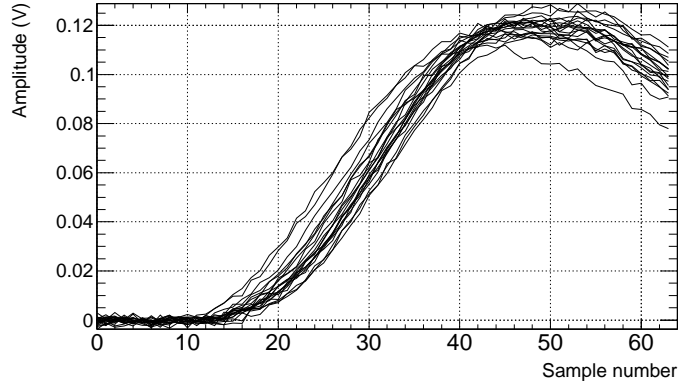


Figure 13: Signals generated by a USFD amplified by a C6-CSA amplifier and acquired by the SAMPIC chip at 3.2 GS/s. Signal properties: 6 ns rising time, laser intensity equivalent to 1 MIP ( $\approx 120$  mV). The signals are interpolated linearly for plotting purposes. The first point is sometimes lost, which is a known feature of the chip related to SAMPIC architecture.

The RMS noise and its fluctuations are of the same order of magnitude than for the previous test, with values ranging from 1.1 to 1.4 mV. However, this time some fluctuations are observed in both the theoretical curve and the experimental measurements. Indeed, the signal being much slower than before, the measurement is also more sensitive to the noise and its fluctuations (see Equation 1). Again the refined CFD allows to get closer to the theoretical curve whereas the CC does even better at low SNR. The jitter of the system is measured to be close to 40 ps in this case.

In Section 6, general conclusions about the tests presented in this paper and plans for future development of the SAMPIC chip are presented.

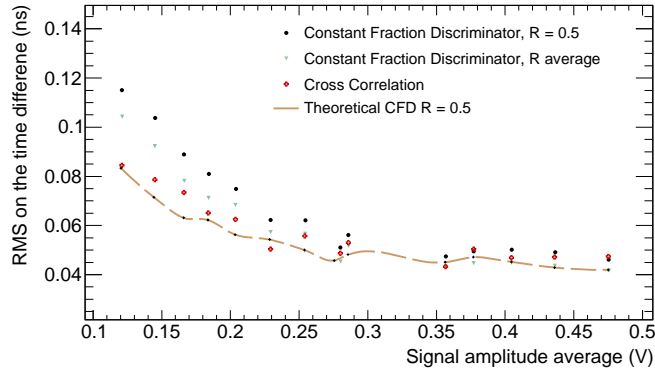


Figure 14: Resolution on the timing measurement of a single channel obtained from the three algorithms implemented in the offline analysis software varying the intensity of the laser pulse. A USFD amplified by a C6-CSA amplifier is used. 120 mV (480 mV) of amplitude in SAMPIC corresponds approximately to the energy deposit of 1 (4) MIP(s) with this experimental apparatus. The fluctuations observed for the theoretical CFD and experimental data are due to small fluctuations of the RMS noise and the slow signals.

## 6. Conclusion

In this article, we reported the first results on the timing measurement resolutions obtained by the SAMPIC V1 chip, which is the version in use as of today. The SAMPIC chip uses an alternative way to measure the time of the input signals, based on fast sampling. In order to analyse SAMPIC data, an online and offline software have been developed to acquire the sampled waveforms and perform accurate timing measurements. In particular, the offline software implements several CFD algorithms and a cross-correlation algorithm which can then be compared. Performance studies of various signal processing algorithms applied on waveform data produced by other digitizers than SAMPIC have already been performed, for example in [27].

The tests were carried out first with ideal signals generated by a signal generator and then with signals from ultra-fast silicon detectors pulsed with an infra-red laser. The resolution was found to be largely independent from the delay between the two signals but showed as expected a significant dependence with respect to the signal amplitudes (*ie.* signal-to-noise ratio). The various results are summarized in Table 2.

At high SNR, all algorithms achieve comparable performance and SAMPIC reaches a resolution of about 4 (40) ps when using synthesized (UFSD) sig-

Sampling frequency	Type of signal	Measurement	Rise time (ns)	CFD resolution (best/worst) (ps)	CC resolution (best/worst) (ps)	Resolution plateau (mV)
6.4 GS/s	Pulse generator	time difference	$\simeq 0.3$	4/27	4/14	> 200
6.4 GS/s	UFSD ( $\simeq 2$ to 4 MIP)	time difference	$\simeq 3$	40/95	40/93	> 300
3.2 GS/s	UFSD ( $\simeq 1$ to 4 MIP)	single channel	$\simeq 6$	40/105	45/85	> 300

Table 2: Summary of the results of the tests performed with the SAMPIC chip reported in this paper.

nals. The difference in resolution observed between synthesized and USFD signal shows that the resolution in the second case is limited by the detector and amplification chain and not by the chip. The best SAMPIC resolution performance reaches a value below 5 ps RMS, in agreement with the design goal. For UFSD signals, no significant decrease of performances was observed when switching from 6.4 to 3.2 sampling frequency given the fairly long rise time of the signals. The computation time on a 2.3 GHz processor including 4 Gb memory has been found to be about 1 ms (100 ms) per event for the CFD (CC) algorithm. However, this time can be decreased drastically if implemented inside FPGAs as reported in [28] where the CFD computation time is only of 10  $\mu$ s. The CC algorithm would also highly benefit from parallel computation.

In addition, the cross-correlation (which is at first order independent from the baseline computation) and refined CFD algorithms show in general better performance at low SNR. This feature could be very useful to improve the resolution of the measurements without changing the apparatus. It also demonstrates the power of signal processing to improve timing measurement performance and encourages a further development of the offline software.

Finally, the resolution plateau of SAMPIC with respect to the amplitude is close to 300 mV for UFSD signals, which should therefore be the aim in the context of the design of a detection chain willing to use the SAMPIC chip.

However, one should keep in mind that the experiment apparatus used

for the SAMPIC tests reported in this paper differs slightly with respect to the potential applications:

- For high-energy physics and medical imaging (PET) applications, the expected signal is arising respectively from charged protons and gamma photons, and not infra-red photons. Therefore, even if the infra-red laser amplitude is tuned to mimic the average deposit charge of a MIP during the tests, the RMS of the charge distribution is expected to be different in case of charged protons. Furthermore, another detector technology than UFSDs is required to detect gamma photons, such as fast scintillating crystals [29] or detectors based on Cerenkov light [30], which will behave differently than UFSDs.
- In order to use SAMPIC in a large scale high-energy physics experiment, important efforts still must be achieved to reduce the dead time. With the version of the chip tested in this paper (SAMPIC V1), the dead time per channel is at least 200 ns. It got the possibility to be reduced to about 50 ns for one following event in the next version (released in December 2015) by using the so called “ping-pong” method (see Section 2). Furthermore, a waveform TDC producing much more data than a standard TDC, the readout system would also need to be designed in a novel way.

As a final conclusion, the SAMPIC V1 chip is ready to be used now and has been proved to be a valuable solution for the read-out of low SNR sensors for precise timing measurements. The low power requirements, the cost per channel and the performance of the proposed system are ideal for embedded systems that need the estimation of the time of a sensor event with a precision of tens of picoseconds, including applications not related to high energy physics.

## 7. Acknowledgments

We thank N. Cartiglia for the assistance in using UFSD sensors. This work has been partially funded by the P2IO LabEx (ANR-10-LABX-0038) in the framework “Investissements d’Avenir” (ANR-11-IDEX-0003-01) managed by the French National Research Agency (ANR).

## References

- [1] Lyndon Evans and Philip Bryant. LHC Machine. *JINST*, 3:S08001, 2008.
- [2] C. Marquet, C. Royon, M. Saimpert, and D. Werder. Probing the Pomeron structure using dijets and  $\gamma$ +jet events at the LHC. *Phys. Rev.*, D88(7):074029, 2013.
- [3] Annabelle Chuinard, Christophe Royon, and Rafal Staszewski. Testing Pomeron flavour symmetry with diffractive W charge asymmetry. 2015.
- [4] Sylvain Fichet, Gero von Gersdorff, and Christophe Royon. Measuring the diphoton coupling of a 750 GeV resonance. 2016.
- [5] Sylvain Fichet, Gero von Gersdorff, and Christophe Royon. Scattering Light by Light at 750 GeV at the LHC. 2015.
- [6] Sylvain Fichet, Gero von Gersdorff, Bruno Lenzi, Christophe Royon, and Matthias Saimpert. Light-by-light scattering with intact protons at the LHC: from Standard Model to New Physics. *JHEP*, 02:165, 2015.
- [7] S. Fichet, G. von Gersdorff, O. Kepka, B. Lenzi, C. Royon, and M. Saimpert. Probing new physics in diphoton production with proton tagging at the Large Hadron Collider. *Phys. Rev.*, D89:114004, 2014.
- [8] E. Chapon, C. Royon, and O. Kepka. Anomalous quartic W W gamma gamma, Z Z gamma gamma, and trilinear WW gamma couplings in two-photon processes at high luminosity at the LHC. *Phys. Rev.*, D81:074003, 2010.
- [9] O. Kepka and C. Royon. Anomalous  $WW\gamma$  coupling in photon-induced processes using forward detectors at the LHC. *Phys. Rev.*, D78:073005, 2008.
- [10] The ATLAS experiment at the CERN large hadron collider. *Journal of Instrumentation*, 3(08):S08003, 2008.
- [11] S. Chatrchyan et al. The CMS experiment at the CERN LHC. *JINST*, 3:S08004, 2008.

- [12] G. Anelli et al. The TOTEM experiment at the CERN Large Hadron Collider. *JINST*, 3:S08007, 2008.
- [13] Nitesh Soni. ATLAS Forward Detectors and Physics. In *Lake Louise Winter Institute: Celebrating 25 years (LLWI 2010) Lake Louise, Alberta, Canada, February 15-20, 2010*, 2010.
- [14] M Albrow et al. CMS-TOTEM Precision Proton Spectrometer. Technical Report CERN-LHCC-2014-021. TOTEM-TDR-003. CMS-TDR-13, CERN, Geneva, Sep 2014.
- [15] Christophe Royon and Nicolo Cartiglia. The AFP and CT-PPS projects. *Int. J. Mod. Phys.*, A29:1446017, 2014.
- [16] C. Royon, M. Saimpert, Kepka O., and R. Zlebcik. Timing detectors for proton tagging at the LHC. *Acta Physica Polonica B, Proceedings Supplement*, Vol. 7, Number 4:735, 2014.
- [17] Manjit Dosanjh, Manuela Cirilli, Steve Myers, and Sparsh Navin. Medical applications at cern and the enlight network. *Frontiers in Oncology*, 6(9), 2016.
- [18] E. Delagnes, D. Breton, H. Grabas, J. Maalmi, and P. Rusquart. Reaching a few picosecond timing precision with the 16-channel digitizer and timestamper SAMPIC ASIC. *Nuclear Instruments and Methods in Physics Research Section A: Accelerators, Spectrometers, Detectors and Associated Equipment*, 787:245 – 249, 2015.
- [19] L Perktold and J Christiansen. A multichannel time-to-digital converter asic with better than 3 ps rms time resolution. *Journal of Instrumentation*, 9(01):C01060, 2014.
- [20] F. Druillole, D. Lachartre, F. Feinstein, E. Delagnes, H. Lafoux, and C. Hadamache. The analogue ring sampler: an asic front-end electronics of the antares neutrino telescope. In *Nuclear Science Symposium Conference Record, 2001 IEEE*, volume 1, pages 138–142 vol.1, Nov 2001.
- [21] Hervé Grabas. *Development of a picosecond time-of-flight system in the ATLAS experiment*. PhD thesis, U. Paris-Sud 11, Dept. Phys., Orsay, 2013.

- [22] JP Lewis. Fast normalized cross-correlation. *Vision interface*, 10(1):120–123, 1995.
- [23] HF-W Sadrozinski, S Ely, V Fadeyev, Z Galloway, J Ngo, C Parker, B Petersen, A Seiden, A Zatserklyaniy, N Cartiglia, et al. Ultra-fast silicon detectors. *Nuclear Instruments and Methods in Physics Research Section A: Accelerators, Spectrometers, Detectors and Associated Equipment*, 730:226–231, 2013.
- [24] N Cartiglia, R Arcidiacono, M Baselga, R Bellan, M Boscardin, F Cenna, GF Dalla Betta, P Fernandez-Martnez, M Ferrero, D Flores, et al. Design optimization of ultra-fast silicon detectors. *Nuclear Instruments and Methods in Physics Research Section A: Accelerators, Spectrometers, Detectors and Associated Equipment*, 796:141–148, 2015.
- [25] G Pellegrini, P Fernández-Martínez, M Baselga, C Fleta, D Flores, V Greco, S Hidalgo, I Mandić, G Kramberger, D Quirion, et al. Technology developments and first measurements of low gain avalanche detectors (lgad) for high energy physics applications. *Nuclear Instruments and Methods in Physics Research Section A: Accelerators, Spectrometers, Detectors and Associated Equipment*, 765:12–16, 2014.
- [26] N. Cartiglia, F. Cenna, A. Picerno, F. Ravera, V. Fadeyev, H. Sadrozinski, A. Seiden, P. Freeman, Z. Galloway, G. Pellegrini, P. Fernández-Martínez, M. BASELGA, V. Greco, S. Hidalgo, D. Quirion, C. Royon, E. Delagnes, M. Saimpert, D. Breton, J. Maalmi, and N. Minafra. Measurement of the Time Resolution of Ultra-Fast Silicon Detectors . In *2014 IEEE Nuclear Science Symposium and Medical Imaging Conference (2014 NSS/MIC), and 21st Symposium on Room-Temperature Semiconductor X-Ray and Gamma-Ray Detectors*, Seattle, United States, November 2014. See Electronique.
- [27] D. Breton, E. Delagnes, J. Maalmi, K. Nishimura, L.L. Ruckman, G. Varner, and J. Va’vra. High resolution photon timing with mcp-pmts: A comparison of a commercial constant fraction discriminator (cfd) with the asic-based waveform digitizers {TARGET} and wave-catcher. *Nuclear Instruments and Methods in Physics Research Section A: Accelerators, Spectrometers, Detectors and Associated Equipment*, 629(1):123 – 132, 2011.

- [28] D. Breton, E. Delagnes, J. Maalmi, and P. Rusquart. The wavecatcher family of sca-based 12-bit 3.2-gs/s fast digitizers. In *Real Time Conference (RT), 2014 19th IEEE-NPSS*, pages 1–8, May 2014.
- [29] E. Auffray, B. Frisch, F. Geraci, A. Ghezzi, S. Gundacker, H. Hillemanns, P. Jarron, T. Meyer, M. Paganoni, K. Pauwels, M. Pizzichemi, and P. Lecoq. A comprehensive amp; systematic study of coincidence time resolution and light yield using scintillators of different size and wrapping. *IEEE Transactions on Nuclear Science*, 60(5):3163–3171, Oct 2013.
- [30] D. Yvon, J. P. Renault, G. Tauzin, P. Verrecchia, C. Flouzat, S. Sharyy, E. Ramos, J. P. Bard, Y. Bulbul, J. P. Mols, P. Starzynski, D. Desforge, A. Marcel, J. M. Reymond, S. Jan, C. Comtat, and R. Trebossen. Calipso: An novel detector concept for pet imaging. *IEEE Transactions on Nuclear Science*, 61(1):60–66, Feb 2014.